

Chapter 13

Creation of Organic-Metal Hybridized Nanocrystals Toward Nonlinear Optics Applications



**Tsunenobu Onodera, Rodrigo Sato, Yoshihiko Takeda,
and Hidetoshi Oikawa**

Abstract Organic nanocrystals are occupied in an intermediate state between single molecule and the corresponding molecular crystal in a bulk state, which are fabricated in common by using the reprecipitation method. The crystal size is in the range of several tens nanometer to sub-micrometer. In particular, linear optical properties such as excitonic absorption spectrum and fluorescence emission spectrum are evidently dependent on crystal size, owing to thermally soften nanocrystal lattice with increasing specific surface area. Core-shell-type hybridization between organic nanocrystals and novel metal nanoparticles is of too much interest in current material science. In this chapter, creation of polydiacetylene nanocrystal fibers hybridized with gold nanoparticles will be introduced in details toward nonlinear optics applications. Polydiacetylene is typically one-dimensional π -conjugated polymer, and one of the most promising organic nonlinear optical materials. It is expected that nonlinear optical properties would be enhanced because of peculiar optoelectronic interaction between exciton in polydiacetylene and localized surface plasmon resonance effect in gold nanoparticles.

Keywords Polydiacetylene · Nanocrystal fiber · Nonlinear optical property · Exciton · Localized surface plasmon resonance

T. Onodera · H. Oikawa (✉)
Institute of Multidisciplinary Research for Advanced Materials (IMRAM), Tohoku University,
Katahira 2-1-1, Aoba-ku, Sendai 980-8577, Japan
e-mail: hidetoshi.oikawa.e8@tohoku.ac.jp

R. Sato · Y. Takeda
Hydrogen Materials Engineering Group, Center for Green Research on Energy and
Environmental Materials, National Institute for Materials Science (NIMS), Sakura 3-13,
Tsukuba 305-0003, Japan

13.1 Introduction

13.1.1 *Scopes of Hybridized Nanomaterials*

Hybridization and/or hybrid on nanometer to sub-micrometer scales, for example, typically polymer blends (polymer alloys), and polymer composites containing inorganic fillers, is one of the most important molecule design concepts and the interesting topics in current materials science and technology [1]. In these hybridized systems, the domain size of each component and its three-dimensional distribution in a polymer matrix would determine mainly the final properties and function, accompanied with selection and combinations of component materials [2]. As a result, the resulting physicochemical properties would become additive and/or intermediate state in the hybridized materials. Especially, organic–inorganic hybridized materials like polymer composites are of too much interest [3], because of emergence of unique nanostructure, and of enhancement of noble physical properties and excellent functions, due to peculiar couplings and interactions at an interface between organic and inorganic components [4].

On the contrary, “hybridized nanomaterials” is on nanometer scale in overall size, and should be essentially different from above-mentioned hybridized materials [5]. The hybridized nanomaterials are in common comprised from metal nanoparticles (NPs) [6], semiconductor quantum dots (SQDs) [7], and magnetic (or inorganic oxides) NPs [8], and have recently attached great attention and interest on nanoscience and nanotechnology. These kinds of NPs themselves provide characteristic properties, e.g., localized surface plasmon resonance (LSPR) [6], quantum confinement effect [7], giant magneto resistive effect [8], and extraordinary polarization field induced by high refractive index [9]. In addition, π -conjugated organic and polymer nanocrystals (NCs) are also one of the candidate components in hybridized nanomaterials [10–12].

13.1.2 *Organic and Polymer Nanocrystals*

Organic and polymer NCs (hereinafter, called organic NCs) are a kind of molecule crystals, and are occupied at an intermediate state between single molecule and the corresponding bulk crystals [10–12]. Organic NCs are usually fabricated by means of so-called reprecipitation method and its developed and/or improved processes, and the crystal size is located in the range between several tens nanometer and sub-micrometers. For example, the acetone (good solvent) solution of diacetylene (DA) monomer is quickly injected into vigorously stirred water medium as a poor solvent, and then the formed DA NCs are solid-state polymerized to convert DA to polydiacetylene (PDA) by UV-irradiation [13]. Here, PDA is a typical one-dimensional π -conjugated polymer, and is one of the most promising organic nonlinear optical

(NLO) materials having high third-order NLO susceptibility and ultra high speed optical response [14, 15].

As a result, one can successfully obtain well-defined PDA NCs dispersed in an aqueous medium [10–12]. The morphology such as crystal size and shape of organic NCs is controlled experimentally by changing reprecipitation conditions: selection of good and poor solvents, concentration and injected amount, injection rate, temperature and stirring rate of poor medium, addition of surfactant, and so on. Organic NCs provide some interesting linear optical properties and function [10–12]. For example, the excitonic absorption peak (EAP) positions are continuously blue-shifted with decreasing crystal size in the case PDA NCs [16], whereas the fluorescence emission peak positions measured with near-field scanning optical microspectroscopy (NSOM) are also blue-shifted in the case of perylene NCs as the crystal size is reduced [17]. These kinds of optical shift are due to thermally soften nanocrystal lattice induced by the increase in specific surface area in small-sized organic NCs, i.e., reduction of optoelectronically inter-molecular interaction in nanocrystal lattice [18]. In addition, the layered thin films have been finely prepared by utilizing negative surface potential of PDA NCs, and then the third-order NLO susceptibility was multiplied apparently with the number of layers toward optoelectronic and/or photonic device applications [10, 11].

13.1.3 Organic-Metal Hybridized Nanocrystals

So far, PDA core-silver (Ag) shell-type hybridized NCs have been fabricated successfully by establishing visible-light-driven photocatalytic reduction method [19], and were characterized carefully with scanning electron microscope (SEM), transmission electron microscope (TEM) with electron diffraction (ED) pattern, powder X-ray diffraction (XRD) pattern, and electron probe X-ray microanalyzer (EPMA).

In fact, the aqueous solution of AgNO_3 and NH_3 was added into PDA NCs dispersion liquids, and then visible (Vis) light was irradiated at a given interval. As a result, it was confirmed that Ag NPs (ca. 10 nm in size) as Ag shell were selectively deposited only on the surface of PDA NCs as a core. The extinction spectrum showed the interesting features, that is, the red-shift and broadening of LSPR peaks from Ag shell, and also red-shifted EAP of PDA core. The former is caused by inhomogeneous distribution in size and the dephasing effect of LSPR, and the later is due to changes of dielectric environment in the surrounding PDA core. The necessitated condition is that the redox potential of metal ion should be located between conduction band (CB) and valence band (VB) of PDA core [18]. Probably, the excited electron at CB would reduce metal ion effectively, and the formed metal NPs are selectively adsorbed only on the surface of PDA core with negative surface potential. In addition, the size and deposition density of the resulting metal NPs were influenced considerably by the relationship between redox potential of metal ion and work function of metal NPs [18, 19]. Actually, one can deposit Ag NPs on the surface of PDA core, being independent of morphology (size and shape) of PDA core [19]. The present concept of formation

mechanism could be basically applied to produce the other kinds of hybridized NCs such as polyalkylthiophene (PAT) core-platinum (Pt) hybridized NCs [20].

On the other hand, Ag core-PDA shell-type hybridized NCs were also produced by using co-precipitation and microwave-irradiation method [21]. In this case, the acetone solution of DA monomer was quickly injected into an aqueous dispersion liquid of Ag NPs, and then DA NCs as a shell were formed well on the surface of Ag NPs as a core. DA shell was converted to PDA shell by UV-irradiation.

In this chapter, a new type of hybridized PDA nanocrystal fibers (NCFs) [22] as a core with gold (Au) NPs as a shell have been created, and nanostructural correlation of optical properties will be discussed in detail. Interestingly, silica thin layer was introduced experimentally between PDA core and Au shell so as to possibly control LSPR effect from Au NPs [23].

13.2 Hybridized Polydiacetylene Nanocrystal Fibers

13.2.1 Preparation of PDA Nanocrystal Fibers

As described in the previous 13.1.2, it is possible to control the morphology of organic NCs by suitably optimizing the reprecipitation conditions. In the case of PDA NCs, the crystal size decreases in general with decreasing the concentration of injected DA-acetone solution [10–12]. On the other hand, the added surfactant and temperature of poor medium would affect remarkably the shape [22]. Actually, the formation of PDA NCFs was confirmed by SEM (JEOL: JSM-6700F) observation (Fig. 13.1). The two kinds of surfactants (SDS: sodium dodecyl sulfate, and CTAB: hexadecyl trimethyl ammonium bromide) were employed and added to DA-acetone solution in advance, and subsequently the injection was performed at the elevated temperature (60 °C) of water medium. The typical diameter is ca. 30–50 nm and the counter length is more than several μm in any resulting PDA NCFs. On the other hand, only PDA NCs were produced around and/or below at room temperature, even though the surfactants were co-existed.

The formation mechanism of PDA NCFs is speculated as follows [10–12]. Probably, amorphous NPs of DA is formed at the initial stage just after injection at the elevated temperature. These amorphous DA NPs are stabilized by the added surfactants, and then the delay in nanocrystallization would occur in individual amorphous DA NPs. Meanwhile, amorphous DA NPs are crystallized to form DA NCs with the elapsed time. At the next stage, already-formed DC NCs may act as a nucleus and/or a kind of substrate, and then another amorphous DA NPs are adsorbed on the facet surface of DA NCs. The adsorbed DA NPs are immediately crystallized through homo-epitaxial-like crystal growth. Consequently, this repetition process could provide one-dimensional DA NCFs, which are solid-state polymerized as usual to produce PDA NCFs. The crystal lattice structure of PDA NCFs was the same as that of PDA NCs by the measurements with powder XRD patterns (Bruker: D8

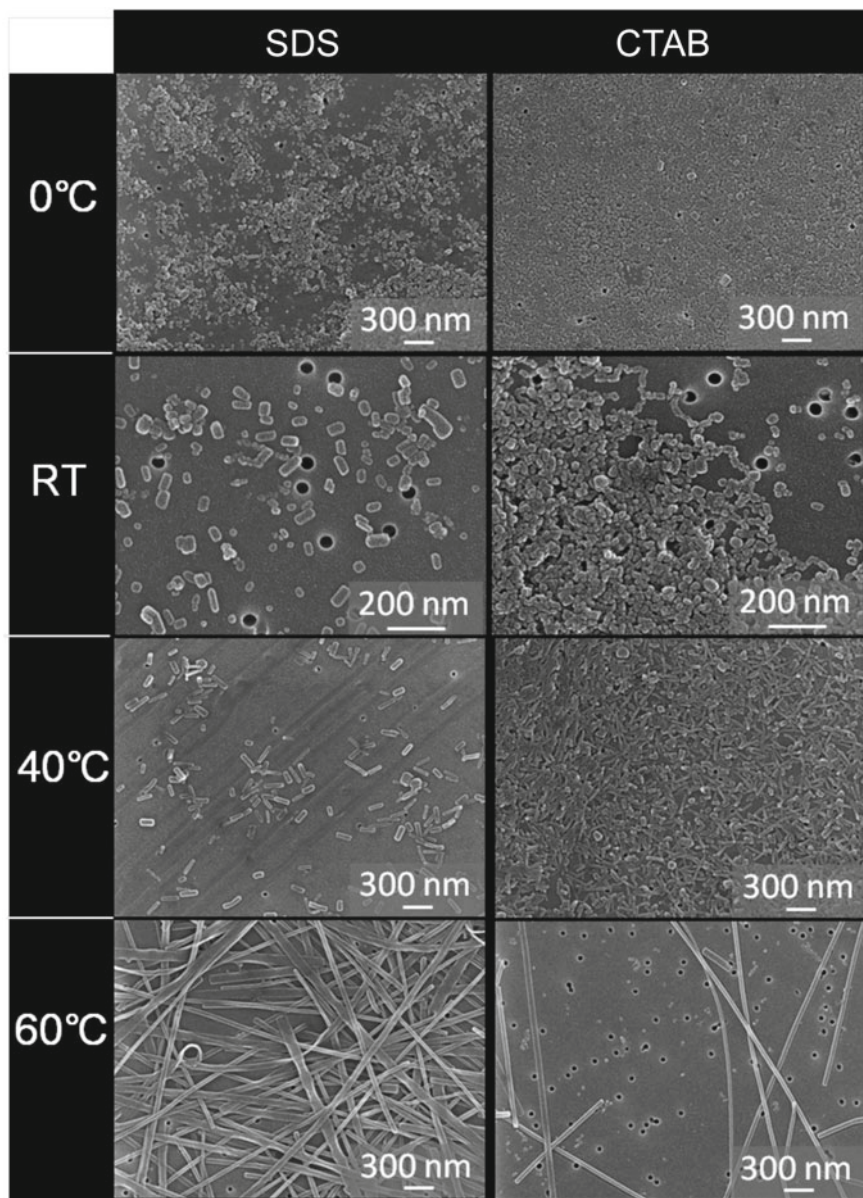


Fig. 13.1 SEM images of PDA NCs and PDA NCFs prepared at various temperatures, when the surfactants, SDS and/or CTAB, were added to acetone solution of DA in the reprecipitation method

ADVANCE) [22]. The surface potential of PDA NCFs is -40 to -60 mV, and PDA NCFs are dispersed stably for half a year in water medium. However, the dispersion stability was not so good in the case of CTAB.

The oriented thin films of PDA NCFs were fabricated easily by means of so-called convective assembly method, which order parameter determined experimentally by the dichroic ratio was high and about 0.87 [22].

13.2.2 Silica Coating of PDA Nanocrystal Fibers

The surface of PDA NCFs was coated with silica layer by using so-called sol-gel method [24], and this layer is much important to control optoelectronic interaction at the interface in the resulting hybridized NCFs [23]. A given amount of EtOH (ethanol), NH_3 , and TEOS (tetraethyl orthosilicate) was added to PDA NCFs dispersion liquid, and then the mixed dispersion liquid was stirred for one hour at room temperature. The small-sized silica NPs were formed at the initial stage and adsorbed locally on the surface of PDA NCFs. After one hour, PDA NCFs were fully coated with silica layer (Fig. 13.2).

The optoelectronic interaction of exciton and LSPR at the interface is intensively dependent on the thickness of silica layer [23, 25, 26]. Namely, it is so important to possibly control the thickness with below 10 nm. However, the thickness of silica layer is estimated to be about 50 nm in Fig. 13.2c, since the diameter of PDA NCFs is 30 nm to 50 nm (Fig. 13.1). However, the trial use of much small amount of TEOS added was unexpectedly ineffective. So, the affinity between surface of PDA NCFs and silica layer has been further improved by employing cationic surfactant (CTAB) and neutral polymer (PEG: polyethylene glycol, $M_w = 3000$) as well as anionic surfactant (SDS). Namely, the sol-gel reaction proceeded under the co-existences of SDS, CTAB, and PEG in PDA NCFs dispersion liquid.

As a result, CTAB was much better to improve the affinity between PDA NCFs and silica layer as shown in SEM images (Fig. 13.3). That is to say, PDA NCFs were almost coated homogeneously with silica layer, when CTAB was used, compared with SDS and PEG. SDS is anionic surfactant, and was not adsorbed enough on

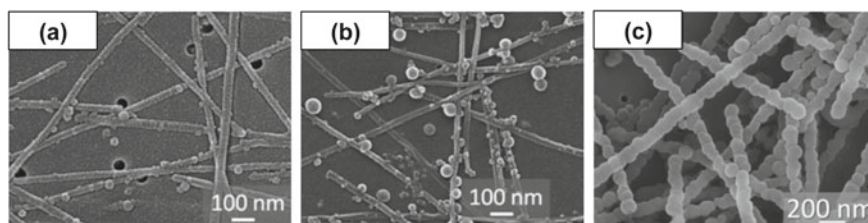


Fig. 13.2 SEM images of silica-coated PDA NCFs by means of sol-gel method. The coating times are **a** 30 min, **b** 40 min, and **c** 60 min

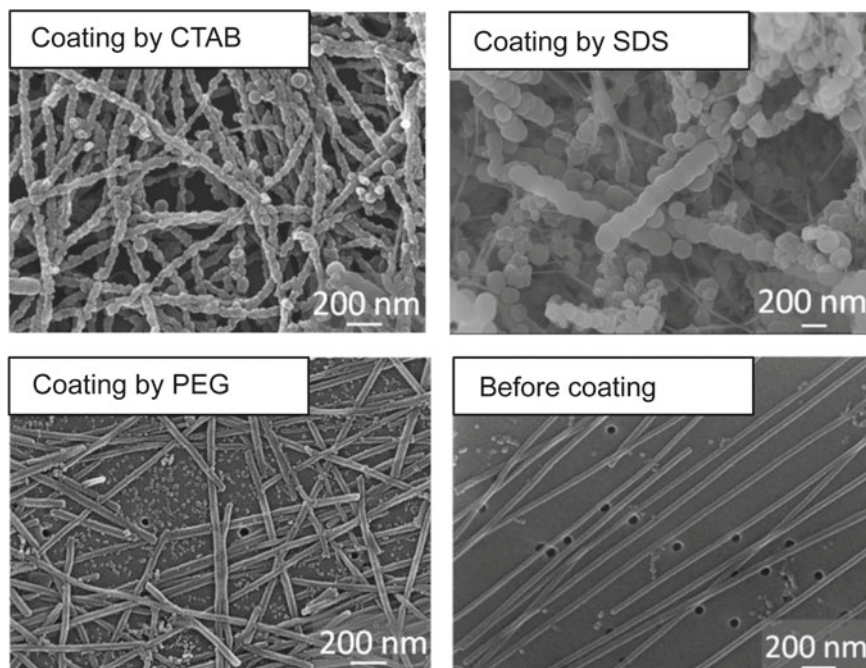


Fig. 13.3 SEM images of silica-coated PDA NCFs fabricated by using various surfactants (CTAB and SDS) and neutral polymer (PEG)

the surface of PDA NCFs, due to electrostatic repulsive interaction. PEG is probably adsorbed somewhat on PDA NCFs. It may be, however, difficult that the formed silica NPs would approach and adsorb subsequently on the surface of PDA NCFs, owing to steric hindrance or conformational repulsion along PEG chains. On the contrary, cationic CTAB may electrostatically interact effectively with both PDA NCFs and silica NPs because of the formation of well-defined bilayer structure having positive charge at both surface sides [27].

Besides the amount of added TEOS and suitably selected CTAB, reaction temperature (Fig. 13.4) and the mixture ratio of water and EtOH (Fig. 13.5) were also experimentally important factors.

These SEM images (Fig. 13.4) show the ones without purification by filtration. Namely, one can see un-adsorbed silica NPs as well as silica-coated PDA NCFs, and discuss qualitatively the temperature effect in the present sol-gel process [24]. The size of silica NPs became smaller with increasing temperature. So, it would be possible to relatively reduce the thickness of silica layer at high temperature.

These SEM images (Fig. 13.5) also exhibit the ones before purification by filtration in order to qualitatively investigate the effect of mixed solvents. The morphology of silica-coated PDA NCFs was changed and influenced remarkably at the various

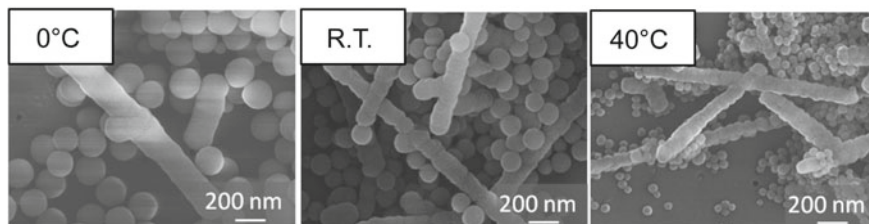


Fig. 13.4 SEM images of silica-coated PDA NCFs prepared at various reaction temperatures, when CTAB was used

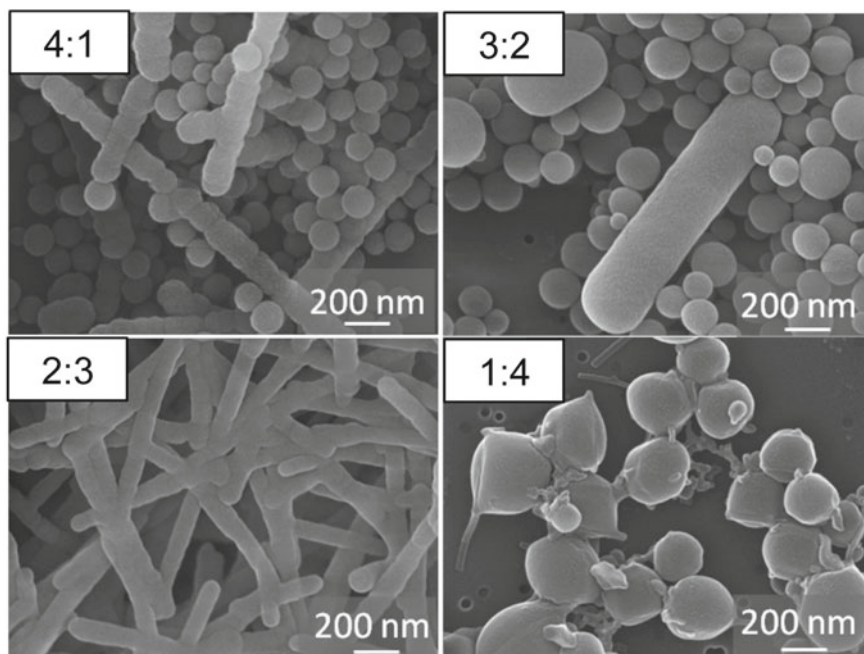


Fig. 13.5 SEM images of silica-coated PDA NCFs fabricated at the different mixture ratios of EtOH and water, EtOH: water = 4:1 to 1:4, when CTAB was also used

ratios of mixed EtOH and water. In common, EtOH added represses the rate of sol-gel reaction [24]. In addition, the critical micelle concentration (CMC) of CTAB in water medium (0.9 mM at 25 °C) is so different from that in EtOH (240 mM at 25 °C) [27]. Probably, these factors strongly affect the thickness of silica layer in the present case. Unexpectedly, it was confirmed from SEM observation that silica-coated PDA NCFs were partially connected each other, when the concentration of CTAB added was more than 10 mM.

Consequently, the silica-coating condition has been optimized successfully so as to fulfill the formation of silica layer with about or below 10 nm in thickness

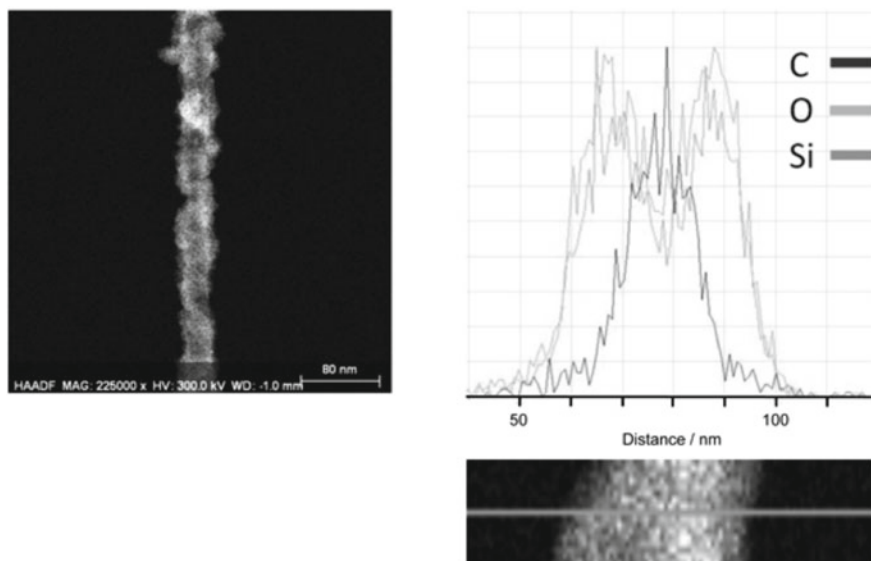


Fig. 13.6 HAADF-STEM image of silica-coated PDA NCFs (left), and the corresponding cross-section profile of elementary mapping (right). C: carbon, O: oxygen, and Si: silicon

on the basis above-mentioned experimental results. Actually, the obtained silica-coated PDA NCFs were characterized precisely with high-angle annular dark field scanning TEM (HAADF-STEM: Titan 80–300 with Image Corrector) observation and the corresponding cross-section profile of elementary mapping (Fig. 13.6). The distributions of oxygen and silicon are almost overlapped in the experimental errors, and the thickness of silica layer is estimated to be about 10 nm. This thickness is approximately comparable with the three-dimensional space distribution in enhanced photoelectric field of LSPR induced at the surrounding noble metal NPs [6, 28, 29], which would be deposited and hybridized on the surface of silica-coated PDA NCFs at the next hybridization step. So far, the emission enhancement of fluorescent dyes induced by LSPR effects has been investigated extensively, depending on thickness of dielectric insulator such as silica layer [25, 26].

13.2.3 Hybridization of PDA Nanocrystal Fibers

PDA core-Ag shell-type hybridized NCs have been fabricated as described in the previous Sect. 13.1.3. The hybridization of silica-coated PDA NCFs as a core and gold (Au) NPs as a shell will be discussed in this sub-section. The LSPR peak of Au NPs ($\lambda_{\text{Au, LSPR}} = \text{ca. } 500\text{--}550 \text{ nm}$) [30] is close to the EAP of PDA (PDA bulk crystal, PDA NCs, and PDA NCFs) ($\lambda_{\text{PDA, EAP}} = \text{ca. } 600\text{--}700 \text{ nm}$, including phonon-side band) [10–12]. So, the strong and peculiar optoelectronic interactions

would be emerged at the core–shell interface [31], rather than Ag NPs ($\lambda_{\text{Ag, LSPR}} = \text{ca. } 390\text{--}400 \text{ nm}$). This would expectedly lead to the enhancement of NLO properties [32], which is due to typically so-called excitation enhancement [23]. The surface of silica-coated PDA NCFs was further modified chemically by using silane-coupling agent (APTES: 3-aminopropyltriethoxysilane), so that amino-functional groups introduced on the surface of silica layer could control the adsorption amounts of Au NPs [33, 34]. After adding Au nano-seed (2–3 nm in size), aqueous solution of Au ion (Au^{3+}) added was reduced mildly by using reducing agent of formaldehyde (HCHO). Here, Au nano-seed was prepared by mixing an aqueous solution containing a given amount of tetrachloroauric (III) acid ($\text{H}[\text{AuCl}_4]$), sodium hydroxide (NaOH), and tertakis(hydroxymethyl)phosphonium chloride (THPC) [35]. On the other hand, aqueous solution of Au^{3+} was obtained by the incubating the mixture of $\text{H}[\text{AuCl}_4]$ aq. and potassium carbonate (K_2CO_3) aq. under dark condition at ca. 5 °C for three days [33]. Furthermore, the previously Pt-sputtered filter substrate was employed, when hybridized PDA NCFs was characterized with SEM observation without using the conventional Pt-sputtering treatment. One can clearly observe the deposited Au NPs, because Au NPs are distinguished from Pt NPs on the filter substrate.

Au NPs have been finely deposited on the surface of amino-terminated silica-coated PDA NCFs, that is, PDA NCFs hybridized with Au NPs, and the deposition amount (or coverage ratio) of Au NPs was controlled and tuned successfully with increasing the injected amount of aqueous solution of Au^{3+} (Fig. 13.7). Interestingly, the size of the deposited Au NPs was not so changed, and only the deposition amount was multiplied. In addition, HAADF-STEM images and the corresponding profile

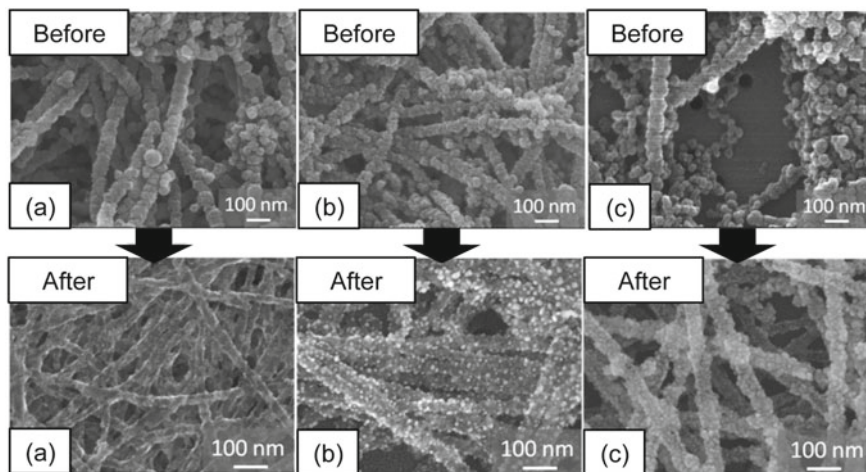


Fig. 13.7 SEM images before and after the deposition of Au NPs as a shell on the surface of amino-terminated silica-coated PDA NCFs. The deposition amounts of Au NPs increased from a–c, and the thickness of silica layer was about 10 nm in any case

of elementary mapping were also observed to further clarify the deposition nanostructure of Au NPs in hybridized PDA NCFs (Fig. 13.8). Au NPs were deposited randomly and almost isolated in the lower coverage ratio, whereas the Au NPs were densely located and connected partially with each other in the case of high coverage ratio.

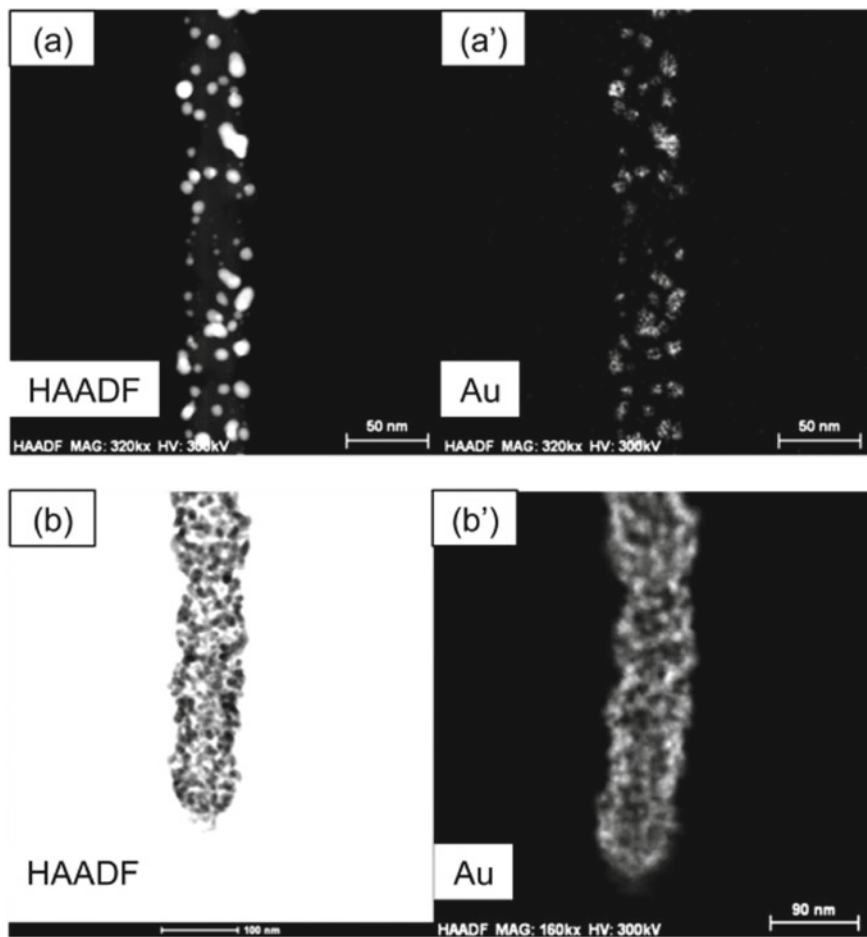


Fig. 13.8 HAADF images, (a) and (b), and the corresponding profiles of elementary mapping of Au, (a') and (b') for Au NPs as a shell deposited on the surface of amino-terminated silica-coated PDA NCFs in the cases of lower, (a) and (a'), and higher, (b) and (b'), coverage ratios

13.3 Optical Properties of Hybridized PDA Nanocrystal Fibers

13.3.1 Solid Thin Films and Linear Optical Properties

It is much important to fabricate well-defined solid thin films of PDA NCFs as well as hybridized PDA NCFs with highly optical quality in order to evaluate linear and nonlinear optical properties, and hybridized nanostructure correlations toward NLO devices applications. PDA NCFs- and/or hybridized PDA NCFs were loaded into polyvinyl alcohol (PVA, DP = 3100, degree of saponification = above 96%) matrix composites thin films in the present study. Actually, an aqueous dispersion liquid of PDA NCFs or hybridized PDA NCFs was mixed with PVA aq., and then water medium was evaporated quickly on a quartz substrate (KU1) around at 100 °C so as to possibly avoid aggregation and orientation. This fabrication process has the advantage to easily produce a large-area thin film without using a large amount of sample dispersion liquid in layer-by-layer method, etc.

The extinction spectra for PVA composites thin films of PDA NCFs or hybridized PDA NCFs were measured with UV–Vis absorption spectrometer (JASCO: V-570) (Fig. 13.9). The extinction spectrum of PVA composites thin film of PDA NCFs shows typically excitonic absorption peak ($\lambda_{\text{PDA, EAP}} = \text{ca. } 650 \text{ nm}$, phonon-side

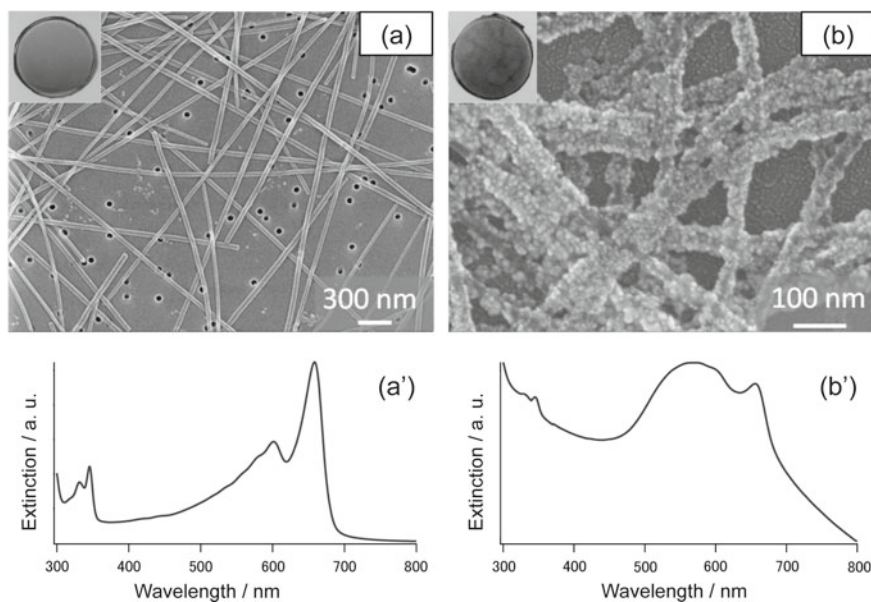


Fig. 13.9 SEM images of PDA NCFs (a) and hybridized PDA NCFs (b), and the corresponding extinction spectra of PVA composites thin film, (a') and (b'). The real color of the photographs of both samples displayed in the insets of (a) and (b) are deep blue and deep black-violet, respectively

band around at 600–630 nm in wavelength). The baseline at above $\lambda = 700$ nm is almost zero. This fact suggests the resulting PVA composites thin film is transparent and highly optical quality with too much less scattering loss. On the other hand, one can see evidently the broad and intensively LSPR peak of deposited Au NPs in the extinction spectrum of hybridized PDA NCFs ($\lambda_{\text{Au, LSPR}} = \text{ca. } 500\text{--}550$ nm) as well as EAP of PDA NCFs.

13.3.2 Pump-Probe Method to Measure Transient Transmission Spectrum for Evaluation of Third-Order NLO Properties

Third-order harmonic generation (THG) method [22] and Z-scan method [14, 18] are conventional techniques to evaluate third-order NLO properties, i.e., $\chi^{(3)}(\omega)$ value. However, the measurements are usually performed discontinuously at a specified wavelength. This is the drawback in these methods. In other words, it is so difficult to measure the wavelength dispersion of $\chi^{(3)}(\omega)$, which would surely bring about the difficulty for discussion about the correlation between $\chi^{(3)}(\omega)$ and nanostructure in the present hybridized systems. Recently, the experimental combination of pump-probe method and spectroscopic ellipsometry has been paid an attention, instead of the previous methods [36–39]. Namely, the wavelength dispersion of real and imaginary parts of $\chi^{(3)}(\omega)$ value is calculated from the difference in complex dielectric function, which is evaluated from experimentally determined wavelength dispersion of complex refractive index and transient transmission spectrum in the present measurement technique.

A pump-probe method was setup for the measurements of transient transmission spectrum (Fig. 13.10). Photo-degradation of PVA composites thin films has been checked from reproducibility of transient component.

13.3.3 Transient Transmission Spectra of PDA Nanocrystal Fibers and Hybridized PDA Nanocrystal Fibers

The transient transmission spectra for PDA NCFs and hybridized PDA NCFs have been measured successfully by using the pump-probe method as described in the previous sub-section (Fig. 13.11). The $\chi^{(3)}(\omega)$ value basically increases with the intensity of transient component, $(\Delta T + T)/T$ [36, 37].

The transient transmission peak appeared strongly at $\lambda = 630\text{--}670$ nm in any cases. Especially, the overall spectral shape in PDA NCFs corresponded to the extinction spectra (Fig. 13.9a). On the other hand, the value of $(\Delta T + T)/T$ unexpectedly became smaller than that of PDA NCFs, although the volume fraction of hybridized PDA NCFs is unclear exactly and not the same as that of PDA NCFs in PVA composites

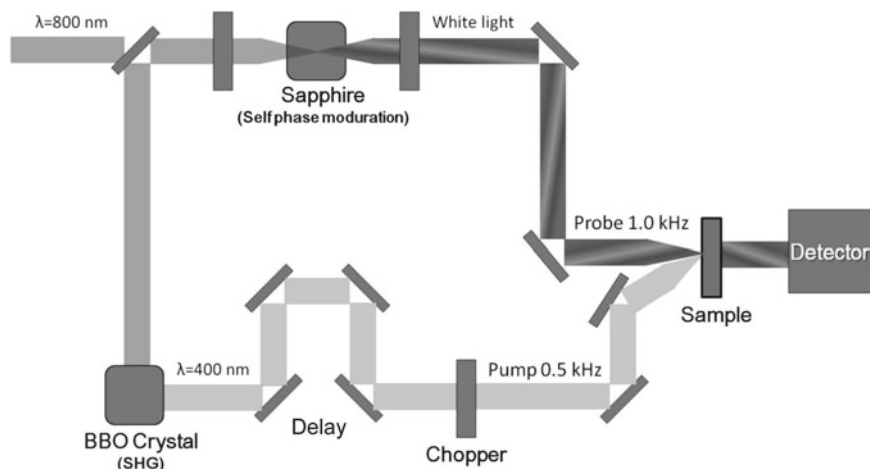
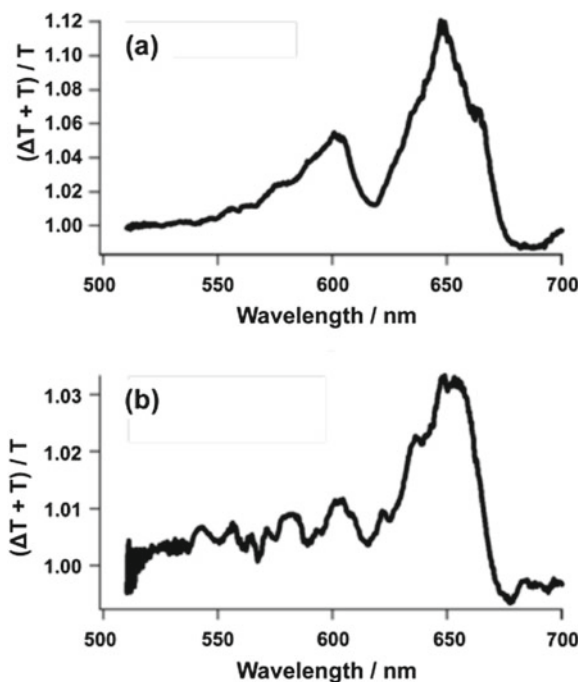


Fig. 13.10 Optical setup in the pump-probe method. Incident pump beam ($\lambda = 800$ nm, 130 fs, and 1 kHz) is launched from laser light source (Spectra-Physics, Inc., Mai-tai and Spitfire with BBO (β -BaB₂O₄) crystal for second harmonic generation (SHG)) consisted of Ti: sapphire laser ($\lambda = 800$ nm, 80 fs, 80 MHz, and above 15 nJ), regenerative amplifier [$\lambda = 800$, 130 fs, 1 kHz, and above 4 mJ), and Nd: YLF (1 kHz, and 20 W)]. The transient transmission spectrum of SrTiO₃ was measured to correct chirping of probe beam, and then the origin of time was revised at individual wavelength

Fig. 13.11 Transient transmission spectra of **a** PDA NCFs and **b** hybridized PDA NCFs with lower coverage ratio of deposited Au NPs



thin film. There are essentially the two main reasons for reduction of $(\Delta T + T)/T$. One is the absorption of incident pump beam by deposited Au NPs (Fig. 13.9b), and the other scattering effect in the hybridized PDA NCFs. In other words, the deposition amount (or coverage ratio) of Au NPs was still excessive even in the case of hybridized PDA NCFs having lower coverage ratio. This fact would provide an important suggestion and guideline for material design of hybridized PDA NCFs. Probably, an extremely small amount of deposited Au NPs is enough to enhance $\chi^{(3)}(\omega)$ value, though no LSPR peak of Au NPs apparently appears in the extinction spectrum. In a word, one should control the deposition number and size of Au NPs, and avoid the aggregation by suitably selecting water-soluble polymers, improving surface modification, and by developing the fabrication processes.

13.4 Conclusions

Aiming at optoelectronic and/or photonic device applications, π -conjugated organic molecules and polymers are the promising NLO materials having high $\chi^{(3)}(\omega)$ value and rapid optical response. Especially, one-dimensional π -conjugated polymer, PDA, is of much interest, which is produced by solid-state polymerization in a crystal state. Morphologically-controlled PDA, that is, PDA NCFs are of great possible to fabricate the corresponding solid thin films, which are an assembled PDA NCFs and regarded as a kind of pseudo-bulk crystal of PDA. However, hybridization of PDA NCFs with noble metal NPs should be needed so as to further enhance $\chi^{(3)}(\omega)$ value. So, the basic fabrication processes, technical issues, and characterization have been investigated in details in this chapter.

The resulting core-shell-type hybridized PDA NCFs with Au NPs have silica layer as a dielectric layer between PDA NCFs as a core and Au NPs as a shell, which layer is important and effective for the purpose of controlling and tuning LSPR effect from Au NPs. Namely, the silica-coating conditions of PDA NCFs were optimized experimentally. Furthermore, the surface of silica layer was chemically modified by introducing amino-function moiety, and then the deposition efficiency of Au NPs was improved considerably.

The transient transmission spectra for PDA NCFs and hybridized PDA NCFs were measured successfully with the pump-probe method. These results and complex refractive index obtained by spectroscopic ellipsometry are fundamental data to precisely evaluate the wavelength dispersion of $\chi^{(3)}(\omega)$. It has become apparent that the deposition amounts of Au NPs were still excessive in the case of hybridized PDA NCFs. One should properly reduce the deposition amounts in the near future. To do so, "polydopamine" will be preferably used at the next objective stage [40], instead of amino-terminate silica layer. In addition, it should be necessary to produce well-defined solid thin films of hybridized PDA NCFs with too much low scattering loss by suitably selecting water-soluble polymers, in addition to PVA, and by optimizing the preparation processes.

Acknowledgements The authors especially thank to the late Professor Emeritus Hachiro Nakanishi in Tohoku University (TU, Japan), Prof. Hitoshi Kasai (IMRAM, TU, Japan), Mr. Y. Hayasaka (technical staff, The Electron Microscopy Center, IMR, TU, Japan), and M.Sc. Rie Chiba (Dept. of Chemistry, Graduate School of Sci., TU, Japan at that time) for their valuable scientific discussion and great experimental contributions.

References

1. Hur, K., Wiesner, U.: Design and applications of multiscale organic-inorganic hybrid materials derived from block copolymer self-assembly. *Adv. Polym. Sci.* **262**, 259–293 (2013)
2. Zhang, S., Pelligra, C.I., Feng, X., Osuji, C.O.: Direct assembly of hybrid nanomaterials and nanocomposites. *Adv. Mater.* **30**, 1705794-1–1705794-23 (2018)
3. Kango, S., Kalia, S., Thakur, P., Kumari, B., Pathania, D.: Semiconductor-polymer hybrid materials. *Adv. Polym. Sci.* **267**, 283–311 (2015)
4. Mai, Y.-W., Yu, Z.-Z.: *Polymer Nanocomposites*. Woodhead Publisher, Cambridge (2006)
5. Ni, W., Yang, Z., Chen, H., Li, L., Wang, J.: Coupling between molecular and plasmonic resonances in freestanding dye-gold nanorod hybrid nanostructures. *J. Am. Chem. Soc.* **130**, 6692–6693 (2008)
6. Loo, C., Lowery, A., Halas, N., West, J., Drezek, R.: Immunotargeted nanoshells for integrated cancer imaging and therapy. *Nano Lett.* **5**, 709–711 (2005)
7. Nomura, M., Kumagai, N., Iwamoto, S., Ota, Y., Arakawa, Y.: Laser oscillation in a strongly coupled single-quantum-dot-nanocavity system. *Nat. Phys.* **6**, 279–283 (2010)
8. Rodrigues, A.R.O., Gomes, I.T., Almeida, B.G., Araujo, J.P., Castanheira, E.M.S., Coutinho, P.J.G.: Magnetic liposomes based on nickel ferrite nanoparticles for biomedical applications. *Phys. Chem. Chem. Phys.* **17**, 18011–18021 (2015)
9. Kuznetsov, A.I., Miroshinichenko, A.E., Brongersma, M.L., Kivshar, Y.S., Luk'yanchuk, B.: Optically resonant dielectric nanostructures. *Science*, **354**, 2472-1–2472-8 (2016)
10. Oikawa, H., Kasai, H., Nakanishi, H.: Fabrication of organic microcrystals and their optical properties (Chap. 11), and Some applications of organic microcrystals (Chap. 12), In: *Anisotropic Organic Materials: Approaches to Polar Order*. ACS Symposium Series 798 (2001)
11. Nakanishi, H., Oikawa, H.: Reprecipitation method for organic nanocrystals (Chap. 2), Optical properties of polymer nanocrystals (Chap. 14), and Particle-based optical devices (Chap. 29). In: *Single Organic Nanoparticles, NanoScience and Technology*. Springer, Berlin (2003)
12. Oikawa, H., Masuhara, A., Kasai, H., Mitsui, T., Sekiguchi, T., Nakanishi, H.: Organic and polymer nanocrystals: their optical properties and function, in nanophotonics: integrating photochemistry, optics and nano/bio materials studies. Elsevier, Amsterdam (2004)
13. Wegner, G.: Solid-state polymerization mechanisms. *Pure Appl. Chem.* **49**, 443–454 (1997)
14. Matsuda, H., Molyneux, S., Kar, A.K., Wherrett, B.S., Okada, S., Nakanishi, H.: Third-order nonlinear optical properties of polydiacetylene crystal. *J. Photopolym. Sci. Technol.* **6**, 261–268 (1993)
15. Giorgetti, E., Margheri, G., Sottini, S., Chen, X., Cravino, A., Comoretto, D., Cuniberti, C., Dell'Erba, C., Dellepiane, G.: Linear and nonlinear characterization of polyDCHD-HS films. *Synth. Met.* **115**, 257–260 (2000)
16. Volkov, V.V., Asahi, T., Masuhara, H., Masuhara, A., Kasai, H., Oikawa, H., Nakanishi, H.: Size-dependent optical properties of polydiacetylene nanocrystals. *J. Phys. Chem. B* **108**, 7674–7680 (2004)
17. Oikawa, H., Mitsui, T., Onodera, T., Kasai, H., Nakanishi, H., Sekiguchi, T.: Crystal size dependence of fluorescence spectra from perylene nanocrystals evaluated by scanning near-field optical microspectroscopy. *Jpn. J. Appl. Phys.* **42**, L111–L113 (2003)

18. Oikawa, H.: Hybridized organic nanocrystals for optically functional materials. *Bull. Chem. Soc. Jpn* **84**, 233–250 (2011)
19. Onodera, T., Oikawa, H., Masuhara, A., Kasai, H., Sekiguchi, T., Nakanishi, H.: Silver-deposited polydiacetylene nanocrystals produced by visible-light-driven photocatalytic reduction. *Jpn. J. Appl. Phys.* **46**, L336–L338 (2007)
20. Onodera, T., Ujita, J., Ishikawa, D., Masuhara, A., Kasai, H., Oikawa, H.: Hybridization of polydiacetylene core and metal shell. *ECS Trans.* **16**, 1–12 (2009)
21. Yokoyama, T., Masuhara, A., Onodera, T., Kasai, H., Oikawa, H.: Development of fabrication process for Ag/polydiacetylene (core/shell) hybridized nanocrystals. *Synth. Met.* **159**, 897–899 (2009)
22. Iimori, Y., Onodera, T., Kasai, H., Mitsuishi, M., Miyashita, T., Oikawa, H.: Fabrication of pseudo single crystalline thin films composed of polydiacetylene nanofibers and their optical properties. *Opt. Mater. Exp.* **7**, 2218–2223 (2017)
23. Naiki, H., Masuhara, A., Masuo, S., Onodera, T., Kasai, H., Oikawa, H.: Highly controlled plasmonic emission enhancement from metal-semiconductor quantum dot complex nanostructures. *J. Phys. Chem. C* **117**, 2455–2459 (2013)
24. Wang, X.D., Shen, Z.X., Sang, T., Cheng, X.B., Li, M.-F., Chen, L.-Y., Wang, Z.-S.: Preparation of spherical silica particles by Stöber process with high concentration of tetra-ethyl-orthosilicate. *J. Colloid Interface Sci.* **341**, 23–29 (2010)
25. Lakowicz, J.R.: Radiative decay engineering 1: Biophysical and biomedical applications. *Anal. Biochem.* **298**, 1–24 (2001)
26. Lakowicz, J.R., Shen, Y., D'Auria, S., Malicka, J., Fang, J., Gryczynski, Z., Gryczynski, I.: Radiative decay engineering 2. Effects of silver island films on fluorescence intensity, lifetimes, and resonance energy transfer. *Anal. Biochem.* **301**, 261–277 (2002)
27. Li, F., Li, G.Z., Wang, H.Q., Xue, Q.J.: Studies on cetyltrimethylammonium bromide (CTAB) micellar solution and CTAB reversed microemulsion by ESR and ^2H NMR. *Colloids Surfaces A Physicochem. Eng. Aspects* **127**, 89–96 (1997)
28. Jin, R.C., Cao, Y.W., Mirkin, C.A., Kelly, K.L., Schatz, G.C., Zheng, J.G.: Photoinduced conversion of silver nanospheres to nanoprisms. *Science* **294**, 1901–1903 (2001)
29. Murphy, C.J., Jana, N.R.: Controlling the aspect ratio of inorganic nanorods and nanowires. *Adv. Mater.* **14**, 80–82 (2002)
30. Chen, S.H., Wang, Z.L., Ballato, J., Foulger, S.H., Carroll, D.L.: Monopod, bipod, tripod, and tetrapod gold nanocrystals. *J. Am. Chem. Soc.* **125**, 16186–16187 (2003)
31. Sakamoto, N., Onodera, T., Dezawa, T., Shibata, Y., Oikawa, H.: Highly enhanced emission of visible light from core-dual-shell type hybridized nanoparticles. *Part. Part. Syst. Charact.* **34**, 1700258-1–1700258-8 (2017)
32. Neeves, A.E., Birnboim, M.H.: Composite structures for the enhancement of nonlinear-optical susceptibility. *J. Opt. Soc. Am. B* **6**, 787–796 (1989)
33. Nghiem, T.H.L., Le, T.N., Do, T.H., Vu, T.T.D., Do, Q.H., Tran, H.N.: Preparation and characterization of silica-gold core-shell nanoparticles. *J. Nanopart. Res.* **15**, 2091-1–2091-9 (2013)
34. Liang, Z.S., Liu, Y., Ng, S.S., Li, X.Y., Lai, L.H., Liu, S.Y.: The effect of pH value on the formation of gold nanoshells. *J. Nanopart. Res.* **13**, 3301–3311 (2011)
35. Shi, W.L., Sahoo, Y., Swihart, M.T., Prasad, P.N.: Gold nanoshells on polystyrene cores for control of surface plasmon resonance. *Langmuir* **21**, 1610–1617 (2005)
36. Sato, R., Momida, H., Ohnuma, M., Sasase, M., Ohno, T., Kishimoto, N., Takeda, Y.: Experimental dispersion of the third-order optical susceptibility of Ag nanoparticles. *J. Opt. Soc. Am. B* **29**, 2410–2413 (2012)
37. Sato, R., Ohnuma, M., Oyoshi, K., Takeda, Y.: Experimental investigation of nonlinear optical properties of Ag nanoparticles: effects of size quantization. *Phys. Rev. B* **90**, 1254171-1–1254171-6 (2014)
38. Sato, R., Ohnuma, M., Oyoshi, K., Takeda, Y.: Spectral investigation of nonlinear local field effects in Ag nanoparticles. *J. Appl. Phys.* **117**, 113101-1–113101-6 (2015)

39. Sato, R., Ishii, S., Nagao, T., Naito, M., Takeda, Y.: Broadband plasmon resonance enhanced third-order optical nonlinearity in refractory titanium nitride nanostructures. *ACS Photonics* **5**, 3452–3458 (2018)
40. Lee, H., Dellatore, S.M., Miller, W.M., Messersmith, P.B.: Mussel-inspired surface chemistry for multifunctional coating. *Science* **318**, 426–430 (2007)